Received: 9 December 2024 | Revised: 3 April 2025 | Accepted: 21 May 2025

DOI: 10.1002/qj.5027

Quarterly Journal of the Royal Meteorological Society RMetS

RESEARCH ARTICLE

Environments of tornadic and non-tornadic supercells in China and optimized significant tornado parameter for China region

Ruqian Zhang[1] | **Ming Xue**[2] | **Xiaoding Yu**[3]

[1]Key Laboratory of Mesoscale Severe Weather/Ministry of Education, School of Atmospheric Sciences, Nanjing University, Nanjing, China

[2]Center for Analysis and Prediction of Storms and School of Meteorology, University of Oklahoma, Norman, Oklahoma, USA

[3]China Meteorological Administration Training Center, Beijing, China

Correspondence
Ming Xue, Center for Analysis and Prediction of Storms and School of Meteorology, University of Oklahoma, Norman, OK 73072, USA.
Email: mxue@ou.edu

Funding information
National Natural Science Foundation of China, Grant/Award Number: 41730965

Abstract

With a sample of 273 supercells spanning 20 years, inflow environment differences between tornadic and non-tornadic supercells in China and its three subregions (northern, central and southern China; CNN, CNC, and CNS) are examined using sounding-derived parameters. Proximity soundings are extracted from the hourly ERA5 reanalysis data. The supercells are categorized as significantly tornadic [rated (E)F2+], weakly tornadic [rated (E)F1], and non-tornadic. Thermodynamic parameters, such as convective available potential energy (CAPE), lifting condensation level (LCL), low-level relative humidity (RH) and convective inhibition (CIN), cannot discriminate between tornadic and non-tornadic supercells effectively. In addition, thermodynamic parameters based on mixed-layer (ML) lifted parcels show worse skill than those for surface-based (SB) or most unstable (MU) lifted parcels. Storm-relative helicity (SRH300) in the range 0–300 m and 0–300-m bulk shear (SHR300) demonstrate greater forecasting skills compared to SRH and shear over deeper depths. Based on predictive skills and distributions of individual parameters, a new significant tornado parameter (STP) formulation, STP300cn, using MUCAPE, MULCL, MUCIN, SRH300, and SHR300 is composed. True skill score (TSS) is used to measure the capability of the individual or combined parameters in discriminating significantly tornadic from non-tornadic supercells. The thresholds and normalization factors for terms in STP are calibrated to the China cases to obtain optimal predictive TSS scores. The calibrated STP parameter, called STP300cn, achieves a TSS of 0.51 in China overall, compared to the 0.14 and 0.29 of the two original versions of STP. It achieves a TSS of 0.37, 0.66, 0.42 for CNN, CNC and CNS, respectively, all much higher than those of the original STP parameters.

KEYWORDS

new tornado parameter, storm environments, supercells, tornado forecasting

1 | INTRODUCTION

Between 1961 and 2010, tornadoes in China caused at least 1772 deaths and resulted in significant damage to property (Fan & Yu, 2015). Most intense tornadoes are associated with supercells but the majority of supercells (at least 70%) do not produce tornadoes (Coffer & Parker, 2015). Observational results have revealed remarkable similarities between tornadic and non-tornadic supercells, including precipitation hook echoes, the presence of low-level mesocyclones (~1 km above ground level [AGL]), occlusion downdrafts and updraft/downdraft structures spiraling cyclonically around the circulations (Coffer & Parker, 2017; Klees *et al.*, 2016; Lemon & Doswell, 1979; Trapp, 1999; Wakimoto *et al.*, 2004; Wakimoto & Cai, 2000).

Although tornadic and non-tornadic supercells have many similarities, proximity soundings and numerical simulations have provided valuable insights into the environmental characteristics and possible mechanisms that distinguish them. Proximity soundings focus on thermodynamic and kinematic parameters such as convective available potential energy (CAPE), lifting condensation level (LCL), and vertical wind shear, examining the characteristics of pre-supercell environments (Brooks *et al.*, 1994; Doswell & Evans, 2003; Mead, 1997; Rasmussen & Blanchard, 1998; Stensrud *et al.*, 1997; Thompson, 1998; Thompson *et al.*, 2003; Weisman & Klemp, 1982). To better understand the relationship between environment parameters and tornado potential, it is useful to review the widely accepted three-step process of tornado formation within supercells: (1) generation of a mid-level mesocyclone (approximately 3–7-km AGL); (2) generation of surface vertical vorticity possibly via downdraft or updraft tilting of horizontal vorticity that is baroclinically or frictionally produced; and (3) contraction of surface vertical vorticity into a tornado and sudden tilting of horizontal vorticity followed by intense stretching (Davies-Jones, 2015; Fischer & Dahl, 2022; Markowski & Richardson, 2014; Rotunno *et al.*, 2017; Schenkman *et al.*, 2014).

In the first step, the updraft, whose strength can be linked to CAPE (Klees *et al.*, 2016), tilts and stretches horizontal vorticity associated with environmental wind shear to generate a mid-level mesocyclone. The mid-level mesocyclone largely results from horizontal streamwise vorticity in the environment (Davies-Jones, 1984). To forecast mesocyclone development, storm-relative helicity (SRH; Davies-Jones *et al.*, 1990) over the inflow vertical range (typically 0–3 km) is preferred over streamwise vorticity because it is far less affected by measurement errors and sampling resolution and takes into account the storm-relative inflow speed (Davies-Jones, 2015). In addition to the 0–3-km SRH, Weisman and Klemp (1982, 1984, 1986) and Weisman (1996) emphasized the importance of strong vertical wind shear over substantial depths, specifically within the 0–4-km or 0–6-km layers. This is because the vertical dynamic pressure forcing needs to extend into the mid-levels of the troposphere to sustain updraft rotation. However, studies using proximity soundings have shown that SRH and vertical wind shear above 1 km are not noticeably different between tornadic and non-tornadic supercells (e.g., Markowski *et al.*, 1998, 2003; Thompson *et al.*, 2003). Apart from observational studies, Coffer *et al.* (2017) using ensemble simulations found that both tornadic and non-tornadic ensemble members contain storms with a strong mid-level updraft. In other words, the formation and intensity of the mid-level mesocyclone may not be the primary factor distinguishing between supercells that produce tornadoes and those that do not. Step 2 is not a sufficient condition for tornado formation either. Simulations by Coffer and Parker (2017) have shown that non-tornadic supercells produced enough vertical vorticity in step 2 but failed to stretch them due to disorganized low-level mesocyclones caused by the ingestion of mainly crosswise horizontal vorticity over the lowest few hundred meters AGL. In contrast, tornadic supercells ingested mostly streamwise horizontal vorticity, leading to a well-organized low-level mesocyclone that effectively enhanced vertical vorticity stretching. Larger SRH over the lowest few hundred meters AGL can enhance the development of a stronger low-level mesocyclone, resulting in more intense dynamic lifting. This dynamic lifting may consequently stretch near surface vertical vorticity, increasing the likelihood of tornadogenesis (Coffer *et al.*, 2017; Coffer & Parker, 2015). Building on this, Coffer *et al.* (2019) made improvements to the significant tornado parameter (STP) in the United States using SRH over the 0–500-m layer AGL. Additionally, Coffer *et al.* (2020) used SRH over the 0–100-m layer AGL to enhance the predictability of STP in both the United States and Europe.

Combined parameters, including bulk Richardson number (BRN; Weisman & Klemp, 1982), vorticity generation parameter (VGP; Rasmussen & Wilhelmson, 1983), energy-helicity index (EHI; Hart & Korotky, 1991), supercell composite parameter (SCP; Thompson *et al.*, 2003) and STP (Thompson *et al.*, 2003) incorporate both kinematic and thermodynamic parameters. Among these combined parameters, STP is one of the most widely used parameters for forecasting tornadic supercells. In addition to 0–1-km SRH (SRH1) and 0–6-km wind shear (SHR6), the earlier version of STP proposed by Thompson *et al.* (2003) also includes mixed-layer (ML, in the lowest 100 hPa) CAPE and MLLCL. Since 2005, the STP has been updated to use surface-based (SB) parcels instead of ML parcels to calculate CAPE and LCL (Coffer *et al.*, 2019). The earlier STP can be called STPfix for the fixed-layer calculation

of kinematic terms. To identify the layers that actually possess CAPE (without excessive values of convective inhibition [CIN]) within the storm inflow, STPfix is further adjusted to use the effective storm inflow layer and effective storm depth for calculations of SRH and bulk wind difference (ESRH and EBWD), respectively, resulting in the effective-layer STP or STPeff (Thompson *et al.*, 2007). Additionally, the CIN term has been added to STPeff to reduce false alarms (Thompson *et al.*, 2011). Thermodynamic terms in STPeff are calculated based on the height of ML. An STP value of 1 serves as a reasonable guideline for distinguishing between significantly tornadic and non-tornadic supercells.

Studies indicate that tornado environments in China significantly differ from those in the United States (Zhang *et al.*, 2023; Zhou *et al.*, 2021). In China, thermodynamic conditions are generally conducive to tornado formation, characterized by moderate to high CAPE and low to moderate LCL. In contrast, kinematic conditions in China are notably less favorable compared to those observed in the United States (Zhang *et al.*, 2023). Therefore, we are interested in whether parameters such as STP still have effective forecasting performance in China? Despite the importance of this question, only a few studies have focused on the differences between tornado and non-tornado storms and their environments in China. Zhou *et al.* (2012) analyzed several cases of tornadic and non-tornadic storms with mesocyclones and found that tornadic mesocyclones had larger values of mesocyclone excess rotational kinetic energy (ERKE; Donaldson & Desrochers, 1990) and lower ERKE-weighted mesocyclone heights than non-tornadic ones. Yu *et al.* (2021) compared environmental parameters characterizing tornadic and non-tornadic supercells in China from 2002 to 2016 using neighboring soundings and surface observations. They found that SHR6 and CAPE could not discriminate tornadic from non-tornadic supercells, while 0–1-km shear and LCL were somewhat able to do so. Their studies did not examine environmental parameters comprehensively or assess the ability of STP to distinguish between tornado and non-tornado events. The limited availability of neighboring soundings at times close to tornado events also affected the generality of conclusions obtained in that study.

This paper utilizes the fifth-generation European Centre for Medium-Range Weather Forecasting (ECMWF) reanalysis (ERA5; Hersbach *et al.*, 2020) that has higher spatial and temporal resolutions compared to other global reanalysis datasets to extract proximity soundings and calculate environmental parameters. With 20-year samples (2002–2021) of tornado and non-tornado supercells, this study aims to identify inflow environment differences between tornadic and non-tornadic supercells using sounding-derived parameters and to examine the predictability of STP in China. Given that recent studies have demonstrated that low-level wind shear exhibits considerable skill in predicting tornadoes (Brooks *et al.*, 2003; Coffer *et al.*, 2019, 2020; Coffer & Parker, 2015, 2017, 2018; Markowski *et al.*, 2003), this study also explores whether using vertical wind shear in a shallower layer can improve the predictive skill of STP for tornadic supercell cases from China. In particular, this study tries to answer the following questions:

1. What are the environmental characteristics of tornadic and non-tornadic supercells in China?
2. How skillful are the two forms of STP (STPfix and STPeff) in predicting tornadoes in China?
3. Can SRH over a shallower layer achieve a greater ability in differentiating between tornadic and non-tornadic supercells in China, similar to findings in America and Europe (Coffer *et al.*, 2019, 2020)?
4. Does shallow-layer vertical wind shear exhibit comparable forecasting skill to shallow-layer SRH?

The rest of this paper is organized as follows. Section 2 describes the methods used in the study, along with the data and regions in detail. Section 3 presents the environmental characteristics of tornadic and non-tornadic supercells. Improvements to the STP in China are illustrated in Section 3.3. Discussion and conclusions about the study are given in Sections 4 and 5.

2 | DATA AND METHODS

The 2002–2021 dataset of tornado and non-tornado cases used in this study comes from four sources. The primary sources are the "Collection of Meteorological Disasters Records in China" (Ding, 2008) and the "Yearbook of Meteorological Disasters in China" (China Meteorological Administration, 2005–2022). Information from meteorological bureaus in China and online sources are also utilized. Furthermore, Doppler radar data are used to confirm that all cases are of the supercell type based on the characteristics of mesocyclone and reflectivity pattern. (E)F0 tornadoes cause minimal damage and are difficult to document comprehensively. Therefore, this study excludes tornadic supercells rated (E)F0. Tornadoes are generally categorized into two types: typical tornadoes and tropical cyclone (TC) tornadoes (less frequent). The environment within TC tornadoes is characterized by higher deep-layer humidity and lower CAPE (Edwards *et al.*, 2012), setting it apart from the environment of typical tornadoes. As a result, TC tornadoes (account for about 10% of total tornado cases examined) are excluded in this paper. Non-tornadic supercells associated with TC

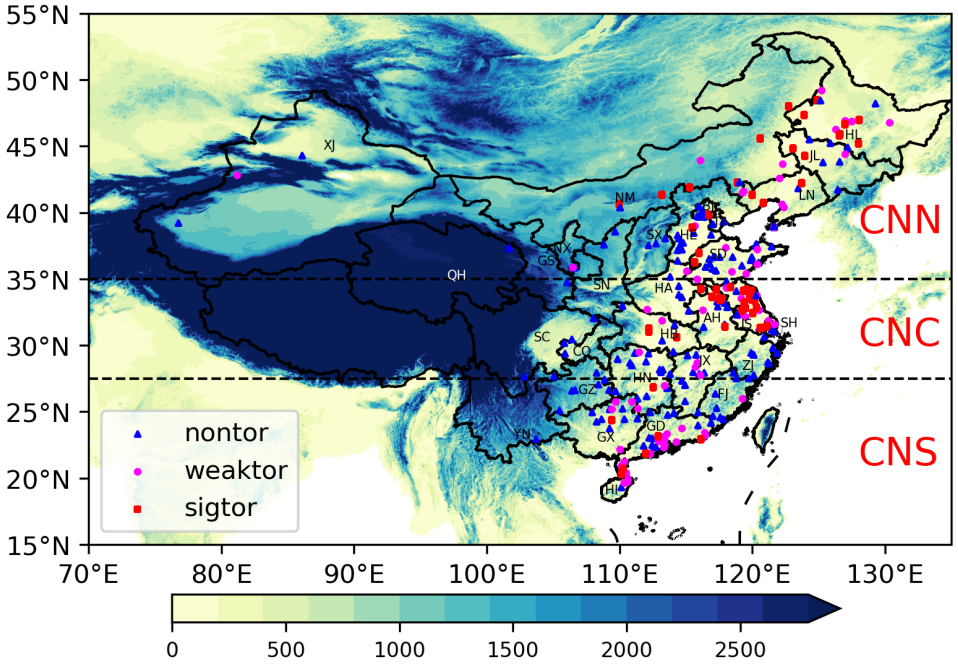

FIGURE 1 Maps of the regional distribution of significantly tornadic supercells (sig-tor), weakly tornadic supercells (weak-tor), and non-tornadic supercells (non-tor) in northern (CNN), central (CNC), and southern China (CNS). The two black dashed lines represent the 35° N and 27.5° N latitude lines, respectively. [Colour figure can be viewed at wileyonlinelibrary.com]

environments are also excluded. Supercells in this paper are categorized as significantly tornadic (sig-tor, rated (E)F2 or greater, 57 cases), weakly tornadic (weak-tor, rated (E)F1, 73 cases), and non-tornadic (non-tor, 159 cases). Most non-tornadic cases collected exhibit severe intensity, characterized by hail larger than 4 mm, strong wind exceeding 20 $m \cdot s^{-1}$, or short-term heavy rainfall. Due to limitations in data records (which are inherently limited and not all examples have precise timestamps or locations) and the distribution of Doppler radar stations in China, the number of non-tornado cases is not significantly greater than that of tornadic cases. However, it is beneficial to have at least comparable sample sizes of tornadic and non-tornadic supercells.

Only a few tornadic and non-tornadic cases are observed in the western regions, such as Xinjiang province (XJ; Figure 1). Tornadic cases are primarily concentrated in the eastern regions of China, while non-tornadic cases are more widely distributed. In addition to their prevalence in eastern China, non-tornadic cases that we collected also extend into topographically complex regions such as Guizhou province (GZ). To exclude the influence of terrain on the environmental differences between tornadoes and non-tornadoes, the 16 non-tornado examples from Guizhou, Yunnan, Sichuan, Chongqing and Qinghai provinces (GZ, YN, SC, CQ, and QH) are excluded from the subsequent analysis. Moreover, to assess the predictive performance of sounding-derived parameters in various regions of China, following Zhang *et al.* (2023), we further divide China into northern (CNN), central (CNC) and southern China (CNS) using latitude lines 35° N and 27.5° N (Figure 1a). The percentages of the three storm types are similar in the CNN and CNC regions, while the number of significant tornado cases we collected is lowest in the CNS region (Table 1). The monthly distribution of each storm type has greater variability than the diurnal distribution (Figure 2). Tornadic supercells are more frequent in summer, with a peak occurrence in July, while non-tornadic supercells tend to occur in spring, peaking in April with a secondary peak in June. Tornadic and non-tornadic supercells exhibit some similarities in their daily distributions, with both being more prevalent in the late afternoon. This overlap makes it more challenging to distinguish them. The collected examples of tornadic and non-tornadic supercells do not exhibit a high degree of spatial and temporal overlap, which may lead to inaccurate statistical results. However, since our focus is on the surrounding environment of supercells themselves, with the high-resolution ERA5 data and the proximity sounding calculation method we used, this study could still provide valuable insights into distinguishing tornadic and non-tornadic supercells in China.

The use of proximity soundings to discern the characteristics of thunderstorms dates back to the 1940s (Beebe, 1958; Fawbush & Miller, 1954; Showalter & Fulks, 1943). These early investigations were conducted using relatively sparse observed soundings. Later, proximity soundings derived from three- or six-hourly radiosonde observations and model analyses were used to explore pre-storm environments (Craven & Brooks, 2004; Evans & Doswell, 2001; Mead, 1997; Rasmussen & Blanchard, 1998; Thompson, 1998). However, due to the often large deviation of the data time from the actual start time of tornadoes, these methods may be less reliable. Recently,

TABLE 1 The number and percentage of significantly tornadic supercells (sig-tor), weakly tornadic supercells (weak-tor) and non-tornadic supercells (non-tor) for northern (CNN), central (CNC), and southern China (CNS)

	CNN		CNC		CNS	
	Number	**Percentage**	**Number**	**Percentage**	**Number**	**Percentage**
Sig-tor	22	21%	28	29%	7	10%
Weak-tor	25	24%	18	19%	30	42%
Non-tor	58	55%	51	53%	34	48%

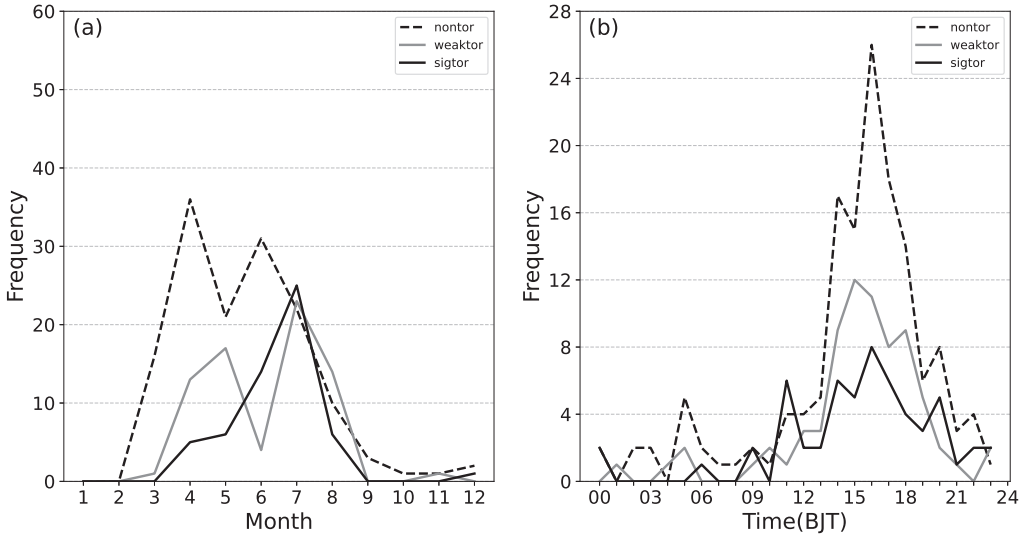

FIGURE 2 Monthly variations (a) and diurnal variations (b) of significantly tornadic supercells (sig-tor), weakly tornadic supercells (weak-tor), and non-tornadic supercells (non-tor) in China.

hourly ERA5 reanalysis data with higher resolution have been applied to such studies (Coffer *et al.*, 2020; Taszarek *et al.*, 2020; Veloso-Aguila *et al.*, 2023; Zhang *et al.*, 2023). Proximity soundings used in this paper are extracted from the ERA5 reanalysis dataset, which has a horizontal spatial resolution of 0.25° and 37 pressure levels in the vertical. While the ERA5 data in the native hybrid sigma-isentropic coordinates offer higher vertical resolution near the ground, those data are harder to download and process. Although the pressure level data are not ideal for calculating shallow-layer SRH and shear, the calculated parameters still show notable predictive skills, as discussed in Section 3.3.2.

The proximity-inflow method employed in this study is described in Zhang *et al.* (2023) and follows the original procedure of Rasmussen and Blanchard (1998). With this method, soundings extracted from the ERA5 are used to represent the inflow environments of the supercell storm events. The sounding corresponding to each event features the closest hourly time before the event. It is within a 100-km radius of the event location and falls within $\pm 75^{\circ}$ of the inflow wind vector. More details can be found in Zhang *et al.* (2023). The sounding-derived parameters are calculated based on the Sounding and Hodograph Analysis and Research Program in Python (SHARPpy), an open-source, cross-platform, upper-air sounding analysis and visualization package (Blumberg *et al.*, 2017). Almost all routines in SHARPpy are written to be as consistent as possible with the methods used at the U.S. National Weather Service (NWS) Storm Prediction Center (SPC).

As mentioned above, STP, which performs well in distinguishing significantly tornadic and non-tornadic supercells in the United States, upgrades from the fixed version to the effective version with respect to the depth over which SRH and BWD are calculated. The formulations of the two versions are.

$$\mathrm{STPfix} = \left(\frac{\mathrm{SBCAPE}}{1500\ \mathrm{J \cdot kg^{-1}}}\right) \times \left(\frac{2000 - \mathrm{SBLCL}}{1000\ \mathrm{m}}\right) \times \left(\frac{\mathrm{SRH1}}{150\ \mathrm{m^2 \cdot s^{-2}}}\right) \times \left(\frac{\mathrm{BWD6}}{20\ \mathrm{m \cdot s^{-1}}}\right), \quad (1)$$

$$\mathrm{STPeff} = \left(\frac{\mathrm{MLCAPE}}{1500\ \mathrm{J \cdot kg^{-1}}}\right) \times \left(\frac{\mathrm{MLCIN} + 200}{150\ \mathrm{J \cdot kg^{-1}}}\right) \times \left(\frac{2000 - \mathrm{MLLCL}}{1000\ \mathrm{m}}\right) \times \left(\frac{\mathrm{ESRH}}{150 \cdot \mathrm{m^2 \cdot s^{-2}}}\right) \times \left(\frac{\mathrm{EBWD}}{20\ \mathrm{m \cdot s^{-1}}}\right). \quad (2)$$

In formulation (1), the SBLCL term is assigned a value of 0.0 when SBLCL exceeds 2000 m, and assigned a value of 1.0 when SBLCL is less than 1000 m. The BWD6 here is the 0–6-km vertical wind shear (Klees *et al.*, 2016). The BWD6 term is set to 0.0 when BWD6 is less than 12.5 $m \cdot s^{-1}$ and set to 1.0 when BWD6 is greater than 30 $m \cdot s^{-1}$. In formulation (2), modifications involve the addition of the MLCIN term and a change in the calculation depth of SRH and BWD parameters, while other aspects remain unaltered. The MLCIN term is assigned a value of 0.0 when MLCIN is less than $-150\ J \cdot kg^{-1}$ and set to 1.0 when MLCIN exceeds $-50\ J \cdot kg^{-1}$.

Significant tornadoes have a high potential for destruction, and this study focuses on evaluating the ability of various parameters to forecast such events. The forecast verification of parameters is through the traditional 2×2 contingency table (Doswell *et al.*, 1990; Doswell & Flueck, 1989) and its associated skill measures. As in Thompson *et al.* (2003), the true skill statistics (TSS), which is also commonly referred to as the Pierce skill score (Peirce, 1884), is used to identify the environmental parameters which are effective in distinguishing between significantly tornadic and non-tornadic supercells. TSS is equal to

$$\mathrm{TSS} = \frac{(ad - bc)}{(a + c)(b + d)}, \tag{3}$$

where a denotes correct forecasts of the event, b denotes wrong forecasts of the non-event, c represents wrong forecasts of the event and d represents correct forecasts of the non-event. The TSS can be interpreted as the disparity between two conditional probabilities in the likelihood-base rate factorization of the joint distribution, namely, the hit rate (POD) and the false alarm rate (POFD; Wilks, 2020). Perfect forecasts are assigned a TSS value of one, random forecasts receive a TSS value of zero and forecasts inferior to the random forecasts get negative scores.

3 | ENVIRONMENTAL CHARACTERISTICS

3.1 | Thermodynamic Parameters

In the United States, both MLCAPE and MLLCL values show a monotonic relationship among storm groups (e.g., significantly tornadic cases have the highest MLCAPE, weakly tornadic cases show intermediate MLCAPE values, non-tornadic cases have the lowest MLCAPE) and when comparing significantly tornadic and non-tornadic supercells, they are proven to be operationally useful (Thompson *et al.*, 2003). In contrast, thermodynamic parameters based on ML lifted parcels exhibit low predictive capability for tornadoes in China (Figure 3). This may be one reason why the original STPeff (discussed in more detail below) shows poor forecasting skills in China.

MLCAPE values for significantly tornadic and non-tornadic supercells differ by nearly one quartile between the 25th and the 75th percentiles of each distribution in the United States (Thompson *et al.*, 2003). However, MLCAPE values for most significantly tornadic cases are lower than those for non-tornadic cases in China (Figure 3a). Yu *et al.* (2021) also found that the distribution intervals of MLCAPE values for tornadic and non-tornadic supercells in China are highly overlapping. Hence, MLCAPE is not a good predictor for tornadic supercells in China ($\mathrm{TSS}_{\mathrm{MLCAPE}} = 0.06$; Table 2). Additionally, parameters derived from the SB and the most unstable (MU, in the lowest 300 hPa) layers are examined. The boxplot of SBCAPE closely mirrors that of MUCAPE, with one slight contrast: the 25th to 75th percentile rank values of MUCAPE for significantly tornadic supercells consistently surpass those for non-tornadic supercells, but it is not so for SBCAPE (Figure 3d,g). From MLCAPE to SBCAPE or MUCAPE, TSS increases from 0.06 to 0.18 (Table 2).

Lower LCL indicates higher relative humidity (RH), potentially leading to enhanced buoyancy in the rear-flank downdraft or inflow and an elevated likelihood of tornado formation (Markowski *et al.*, 2002). MLLCL in China has similar characteristics between significantly tornadic and non-tornadic supercells (Figure 3b). In contrast, the percentile-ranked values of MLLCL in the United States demonstrate a great difference (more than one quartile) between significantly tornadic and non-tornadic supercells (Thompson *et al.*, 2003). In addition, MLLCL in China seems to lack any correlation with the storm types. The TSS value of MLLCL is 0.19 (Table 2), which is greater than the TSS value of MLCAPE. Besides, the median value of MULCL for tornadic supercells is moderately lower compared to that of non-tornadic supercells (Figure 3e). SBLCL has a similar distribution to MULCL (Figure 3e,h). Both SBLCL and MULCL achieve a TSS value of 0.29 (Table 2).

Supercells producing significant tornadoes tend to have less CIN than non-tornadic supercells (Davies, 2004; Rasmussen & Blanchard, 1998). The physical explanation is that large CIN may inhibit the ascent and stretching of low-level parcels, reducing the probability of tornadoes (Davies, 2004). However, CIN is not useful either in distinguishing tornadic and non-tornadic supercells in China. The TSS value of CIN is always around 0.1 regardless of the calculation depth (Table 2). As shown in Figure 3c,f,i (displaying absolute CIN values), the boxplots of CIN for significantly tornadic supercells largely overlap with those for non-tornadic supercells, and weakly tornadic supercells have the lowest median of CIN. The median CIN for

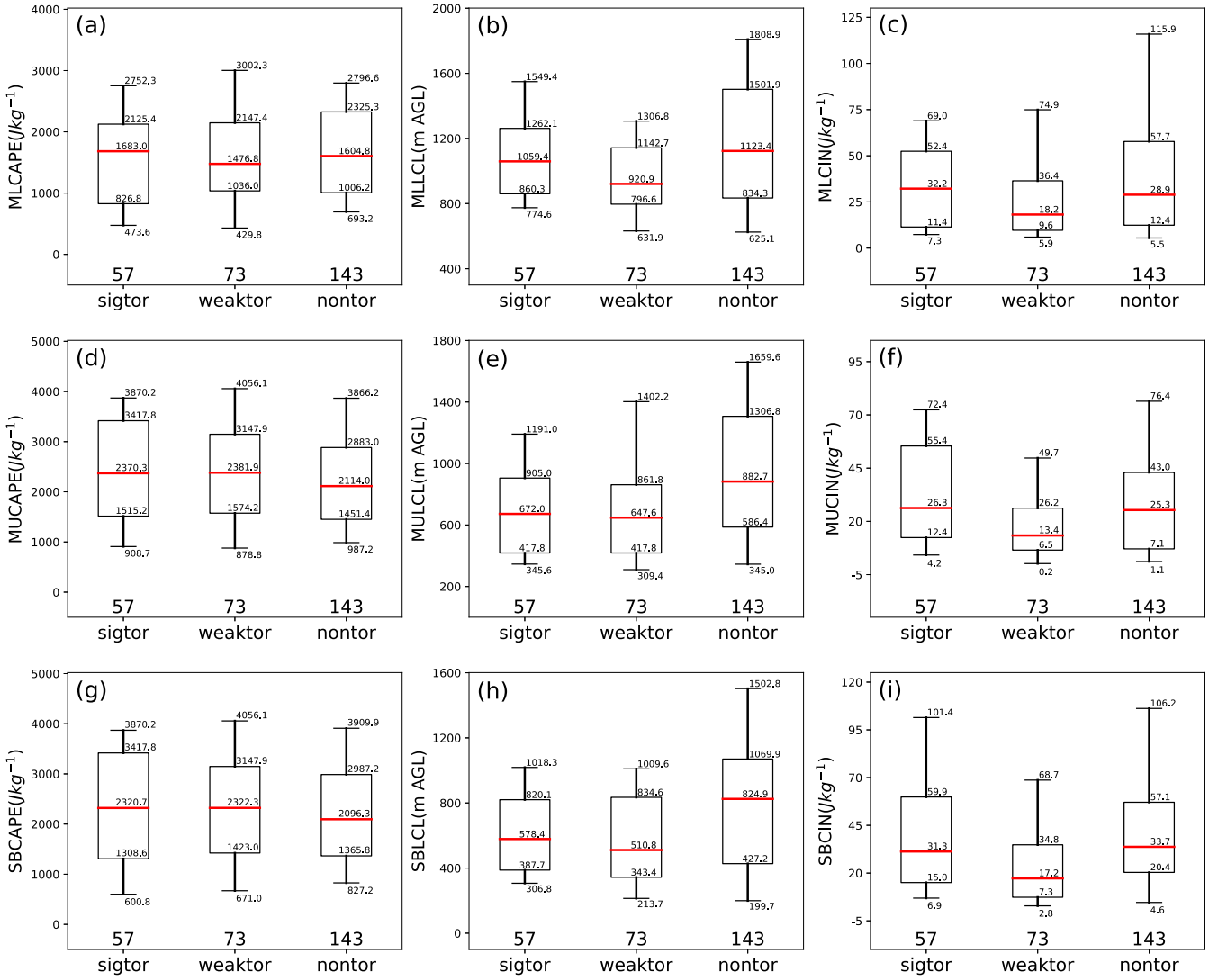

FIGURE 3 Box-and-whisker plots of (a) MLCAPE, (b) MLLCL, (c) the absolute values of MLCIN, (d) MUCAPE, (e) MULCL, (f) the absolute values of MUCIN, (g) SBCAPE, (h)SBLCL, and (i) the absolute values of SBCIN for significantly tornadic supercells (sig-tor), weakly tornadic supercells (weak-tor), and non-tornadic supercells (non-tor). The median value for each category is represented by a red line within the box. The boxes span the 25th–75th percentiles and the whiskers extend to the 10th and 90th percentiles. The numbers of cases for each group are listed below the columns. [Colour figure can be viewed at wileyonlinelibrary.com]

non-tornadic supercells in China is lower than that in the United States (Davies, 2004). Absolute values larger than 50 J · kg^{-1} can be viewed as large CIN. In China, only about 25% of non-tornadic supercells occur with CIN larger than 50 J · kg^{-1} (Figure 3c,f,i). These characteristics of CIN may explain its limited forecasting ability in China.

The forecast skill of thermodynamic parameters varies regionally. One notable fact is that, across three regions, thermodynamic parameters in CNN typically score lower values (Table 3). With TSS values hovering around 0.1 (Table 3), CAPE proves to be the least effective parameter in the CNN region. The cold vortex serves as the primary synoptic background for tornadoes in CNN (Zheng, 2020). Tornadoes occurring under this environment typically exhibit lower CAPE values, a result of reduced low-level moisture and a shallower moist layer (Wang *et al.*, 2015). The poor performance of thermodynamic parameters in the CNN region may be attributed to the characteristics of supercells within cold vortices, which tend to have lower CAPE, drier conditions, and larger CIN, making it difficult to distinguish between tornadic and non-tornadic supercells (Table 3). For tornadoes in the CNN region, kinematic parameters play more important roles, which will be discussed further later. Thermodynamic parameters generally perform better in the CNS region, with the exception of LCL, which has a lower TSS value of ~0.1–0.2 compared to the CNC region (Table 3). The poor performance of LCL is attributed to the overall humid environment in the CNS

TABLE 2 The maximum true skill score (TSS) and the optimal threshold for specific forecasting parameters differentiate significantly tornadic supercells from non-tornadic supercells in China.

	Max TSS	Optimal threshold
MLCAPE	0.06	1698.1
SBCAPE	0.18	2858.1
MUCAPE	0.18	2859.1
MLLCL	0.19	1350.2
SBLCL	0.29	828.2
MULCL	0.29	827.4
MLCIN	0.10	−109.3
SBCIN	0.10	−19.2
MUCIN	0.05	−107.5
lowRH	0.15	75.3
LR85	0.01	8.2
LR75	0.02	8.0
ESRH	0.29	75.7
SRH1	0.34	58.8
SRH300	0.48	10.4
SHR6	0.06	30.0
EBWD	0.01	31.8
SHR300	0.48	2.3
EHI	0.26	0.9
VGP	0.17	0.2
BRN	0.07	31.6
SCP	0.18	11.5
STPfix	0.29	0.5
STPeff	0.14	0.7
STP300cn	0.51	1.0

Note: TSS is computed across 1000 evenly distributed thresholds of the entire ERA5 sounding dataset for each variable.

region, resulting in similarly low LCL values for both tornadic and non-tornadic supercells. In contrast, CAPE and CIN achieve better scores in the CNS region (Table 3), indicating that the tornado in this region does benefit from favorable environmental thermodynamic conditions. Supercells located in CNC are not constrained by regional humidity and achieve the highest LCL scores (~0.4–0.5; Table 3). Associated with relatively high TSS values of CAPE and CIN (Table 3), significant tornadoes benefit most from favorable thermodynamic condition in the CNC region, likely due to the larger variability in environmental humidity and temperature conditions in the region. Besides, thermodynamic parameters based on SB or MU lifted parcels both perform better than ML lifted parcels in the CNC region (Table 3).

Figure 4 shows the composite soundings of significantly tornadic, weakly tornadic, and non-tornadic supercells. To avoid the over-smoothing effect, the soundings in Figure 4 employ the realignment method described in Section 3.2. In China, the low-level environments are warm for all three storm types due to their similar diurnal variance, wetter for weakly tornadic supercells, and drier for both significantly tornadic and non-tornadic supercells (Figure 4). Low-level RH could not distinguish significantly tornadic and non-tornadic clearly (i.e., $TSS_{lowRH} = 0.15$; Table 2). Unlike low-level RH, mid-to-high-level RH is clearly higher in tornadic supercells compared to non-tornadic supercells (Figure 4). The positive CAPE areas on the skew T diagram of different storm types are similar, albeit with a slightly higher average value of CAPE for non-tornadic supercells (Figure 4). Besides, other thermodynamic parameters including 850–500 hPa lapse rate (LR85), 700–500 hPa lapse rate (LR75), and level of free convection (LFC) show limited ability to forecast tornadoes. This is supported by the average values of these parameters shown in Figure 4, which either demonstrate similarities or lack a monotonic relationship among storm groups.

Clearly, thermodynamic parameters perform poorly in predicting tornadoes in China. However, shallow-layer SRH and shallow-layer shear could potentially serve as effective discriminators between tornadic and non-tornadic supercells. We will discuss this in the next subsection.

3.2 | Kinematic Parameters

In China, the median of 0–1-km AGL SRH (SRH1) for significantly tornadic supercells is almost 2.5 times larger than that for non-tornadic supercells (Figure 5b). The median of ESRH for significantly tornadic is 1.5 times larger than that for non-tornadic supercells (Figure 5c). Additionally, ESRH does not exhibit a monotonic relationship across storm groups. In other words, the distribution of ESRH for weakly tornadic supercells is similar to that for non-tornadic supercells (Figure 5c). Therefore, SRH1 has better forecast skill than ESRH. About 95% of supercells in this study are surface-based (i.e., the bottom height of effective inflow is zero) and the median depth of the effective inflow layer is about 1922 m, which is deeper than the depth of SRH1. A shallower layer of SRH may have a greater performance (e.g., SRH1 performs better than ESRH). As shown in Figure 5a, 0–300-m AGL SRH (SRH300) has the best predictive ability among SRH over other layer depths. The 25th percentile of SRH300

TABLE 3 As in Table 2, but for the regions divided in Figure 1.

	CNN		CNC		CNS	
	Max TSS	Optimal threshold	Max TSS	Optimal threshold	Max TSS	Optimal g g g tb
MLCAPE	0.07	2703.8	0.17	1433.6	0.25	1386.4
SBCAPE	0.05	60.3	0.27	3206.1	0.28	2742.6
MUCAPE	0.02	3771.4	0.28	2264.7	0.28	2740.9
MLLCL	0.25	1278.7	0.35	1186.7	0.10	828.1
SBLCL	0.22	919.0	0.54	697.6	0.13	345.8
MULCL	0.24	990.6	0.54	824.6	0.19	347.0
MLCIN	0.16	−88.2	0.08	−17.1	0.32	−41.0
SBCIN	0.13	−88.6	0.15	−20.5	0.27	−31.8
MUCIN	0.12	−98.2	0.15	−20.6	0.21	−31.7
SRH1	0.40	54.4	0.50	52.7	0.25	138.0
ESRH	0.37	75.8	0.40	69.4	0.08	146.5
SRH300	0.51	13.0	0.63	24.4	0.25	19.1
SHR6	0.16	15.0	0.06	15.6	0.14	33.1
EBWD	0.12	19.0	0.05	10.8	0.02	27.0
SHR300	0.50	2.3	0.57	3.4	0.42	1.1
STPfix	0.27	0.4	0.51	0.5	0.08	2.5
STPeff	0.06	1.3	0.38	0.5	0.00	0.0
STP300cn	0.37	1.4	0.66	1.3	0.42	1.0

for significantly tornadic supercells roughly matches the 75th percentile of SRH300 for non-tornadic supercells (Figure 5a). Evidently, SRH300 gets a high TSS value of 0.48 (Table 2). SRH1 follows SRH300 with a lower TSS (0.34; Table 2), while ESRH achieves the lowest score (0.29; Table 2). Compared to the deeper layers used traditionally in operations, increasingly shallower layers of SRH result in increased forecast skill. Variances also exist across different regions in China. CNC, which has the best thermodynamic discrimination capability, consistently demonstrates superior SRH forecasting ability, regardless of the calculation depth of SRH (Table 3). Next to CNC in terms of SRH performance is CNN, with a score difference of only around 0.1 (Table 3). This further suggests that kinematic environmental conditions have more effect on significant tornadoes in CNN. Consistently, SRH300 scores highest compared to other depths of SRH in these two regions. However, SRH performs worse in the CNS region, with ESRH achieving the lowest TSS value of 0.08 (Table 3). The lower SRH scores in CNS, compared to other regions, can be attributed to the relatively low horizontal streamwise vorticity in the region's environment (not shown). This is also a key factor contributing to the lowest proportion of significant tornadoes (excluding TC tornadoes) in CNS, as shown in Table 1.

In China, the vertical wind shear over a deeper depth (SHR6 and EBWD) also shows poor forecasting skills. The median values of SHR6 and EBWD for significantly tornadic supercells are slightly lower than those for non-tornadic supercells (Figure 5e,f), consistent with the findings of Yu *et al.* (2021), who observed similar SHR6 distributions in China. Switching from a fixed-layer to an effective-layer calculation of deep shear does not enhance tornado forecasting performance ($TSS_{SHR6} = 0.06$, $TSS_{EBWD} = 0.01$; Table 2). SHR6 and EBWD can discriminate between supercells and non-supercells, but not tornadic and non-tornadic supercells (Thompson *et al.*, 2003, 2007). In contrast, the median of 0–300-m AGL bulk shear (SHR300) for significantly tornadic supercells is almost four times higher than that for non-tornadic supercells (Figure 5d). In line with this, the TSS value of SHR300 is significantly higher ($TSS_{SHR300} = 0.48$; Table 2). Low-level shear contributes to strengthening, widening, and lowering of the base of the mesocyclone, inducing stronger dynamic lifting that could forcibly lift low-level flow with appreciable vorticity

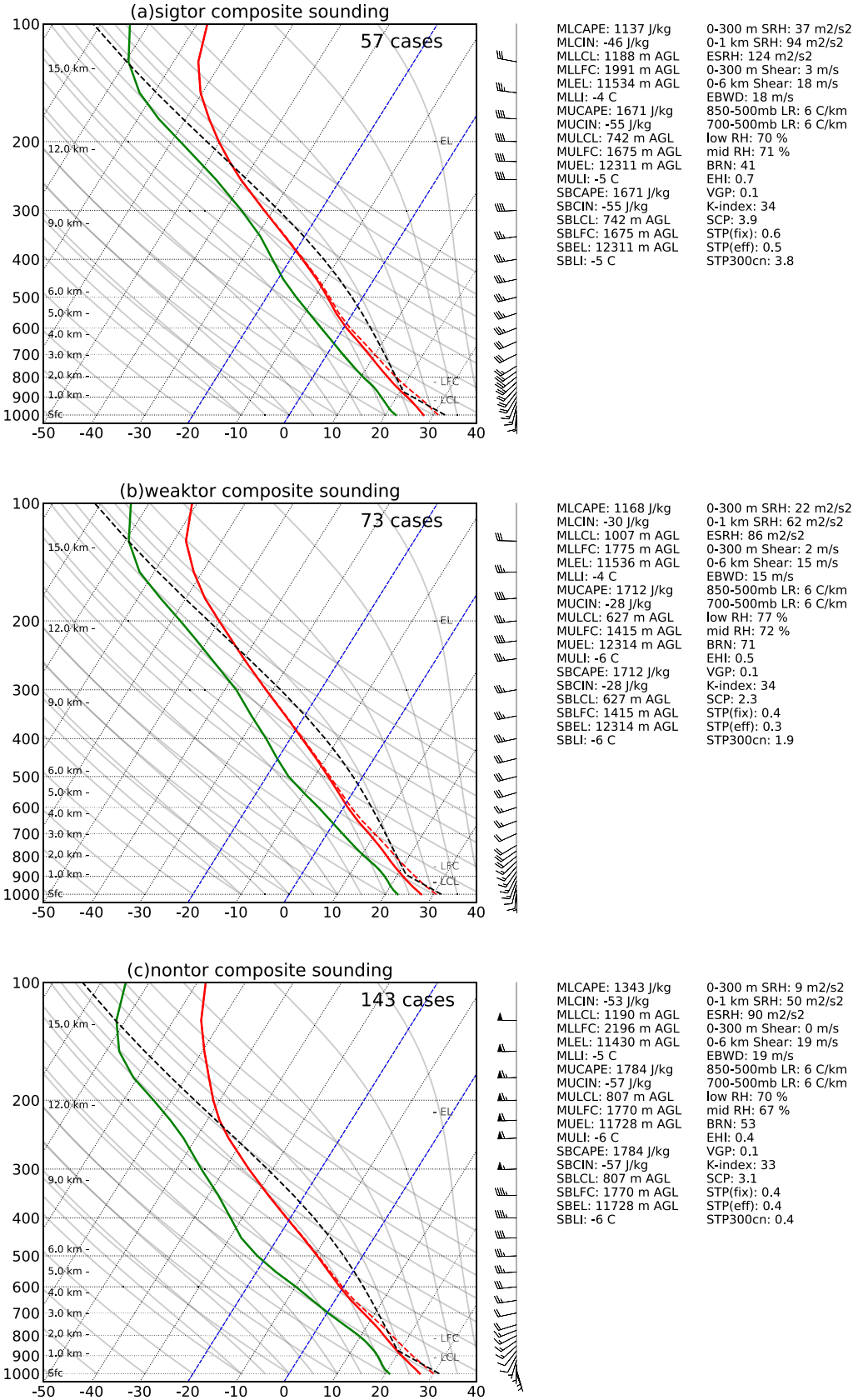

FIGURE 4 Composite soundings of (a) significantly tornadic supercells (sig-tor; 57 cases), (b) weakly tornadic supercells (weak-tor; 73 cases), and (c) non-tornadic supercells (non-tor; 143 cases). Solid red, solid green, dashed red and dashed black lines denote temperature, dewpoint, virtual temperature, and parcel trace. Dashed blue lines denote 0 and −20°C isotherms. The composite wind profile for each region is the average of individual wind profiles after their 0–6-km shear vector is aligned with the mean 0–6-km shear vector. Mean values of different parameters are shown on the right. [Colour figure can be viewed at wileyonlinelibrary.com]

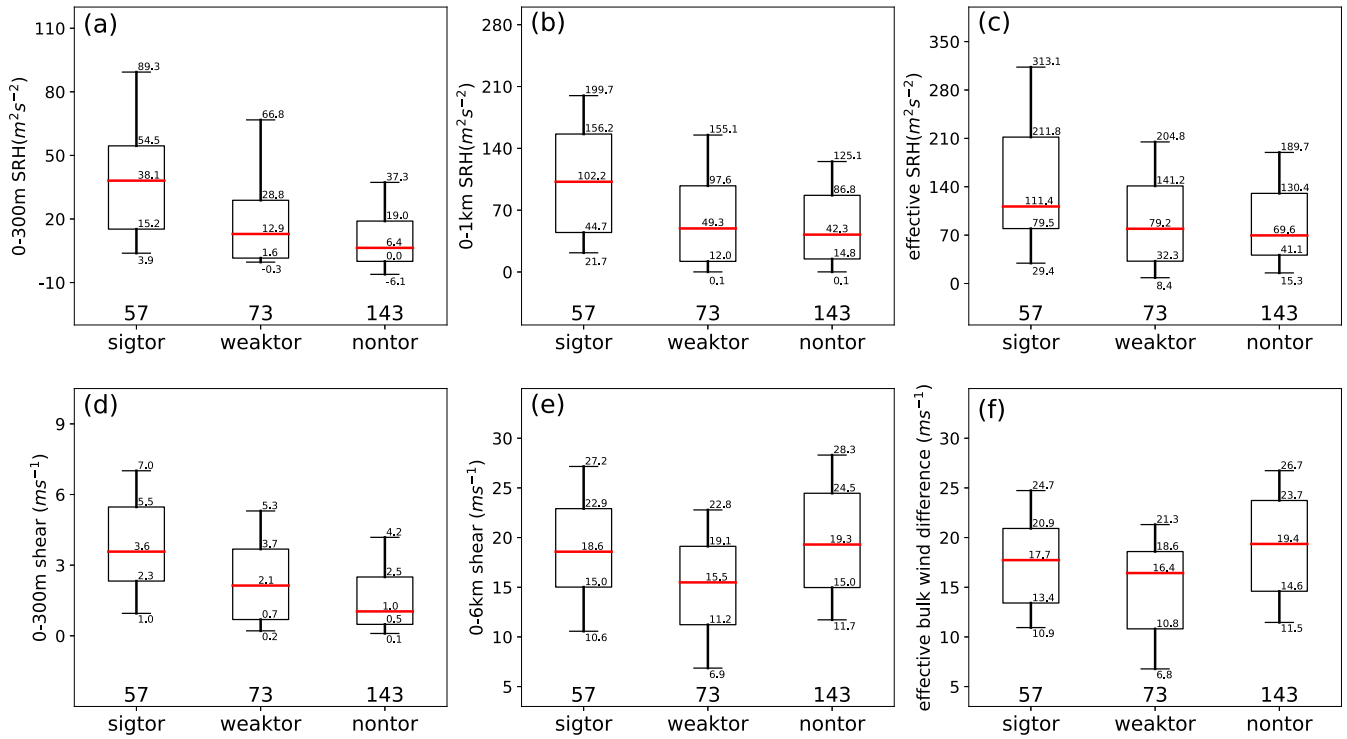

FIGURE 5 Box-and-whisker plots of (a) SRH300, (b) SRH1, (c) ESRH, (d) SHR300, (e) SHR6, and (f) EBWD for significantly tornadic supercells (sig-tor), weakly tornadic supercells (weak-tor), and non-tornadic supercells (non-tor). Other descriptions are as in Figure 3. [Colour figure can be viewed at wileyonlinelibrary.com]

(Coffer & Parker, 2015). This study further demonstrates that shallow-layer shear has a great ability to forecast tornadic supercells, as does shallow-layer SRH. The variance of bulk shear across geographic regions is similar to that of SRH. The CNC region often experiences varying weather systems from the north and south, and prior to strong northwesterly upper-level flows overlaying strong low-level southerly flows, resulting in great wind shear conditions. Specifically, for SHR300, CNC achieves the highest value of 0.57, while CNN and CNS attain values of 0.50 and 0.42, respectively (Table 3). For significant tornadoes in the CNS region, wind shear proves to be a more effective parameter compared to SRH. Additionally, the TSS values for kinematic parameters in the CNS region are lower than those observed in other regions. This discrepancy may be attributed to the relatively weak wind shear environment in the CNS region. Nevertheless, SHR300 remains the most effective differentiator among individual kinematic and thermodynamic parameters in CNS.

To explore the vertical wind shear characteristics among different types of storms, composite hodographs are presented in Figure 6. To prevent over-smoothing from obscuring the original characteristics of the 0–6-km wind shear vector, which may exhibit varying orientations, this paper employs the same realignment method as Zhang *et al.* (2023). The dashed black curve in each panel denotes the composite hodograph without realignment, while solid red represents the composite hodograph after all individual hodographs are first realigned based on 0–6-km shear before averaging. The dashed black and the solid red of the hodograph for each storm type are quite similar, indicating that most cases have similar 0–6 km shear orientations (Figure 6). The low-level shear in three composite hodographs all exhibits clockwise rotation, with significantly tornadic supercells showing the largest curvature (Figure 6). In particular, accompanied by a notable increase in the southerly component, the composite hodograph of significantly tornadic supercells from 0 to 300 m has a corresponding increase (Figure 6a). In sharp contrast, the composite hodograph of non-tornadic cases from 0 m to 300 m remains nearly constant (Figure 6c). Besides, unlike the nearly identical shapes of composite hodographs at higher levels in the United States (Coffer *et al.*, 2020), the shapes of tornadic and non-tornadic hodographs above 6 km in China are different (Figure 6). The hodograph of non-tornadic supercells above 6 km displays a significant increase in the westerly component. This may be attributed to the relatively strong supercell intensity of the non-tornado cases collected in this paper.

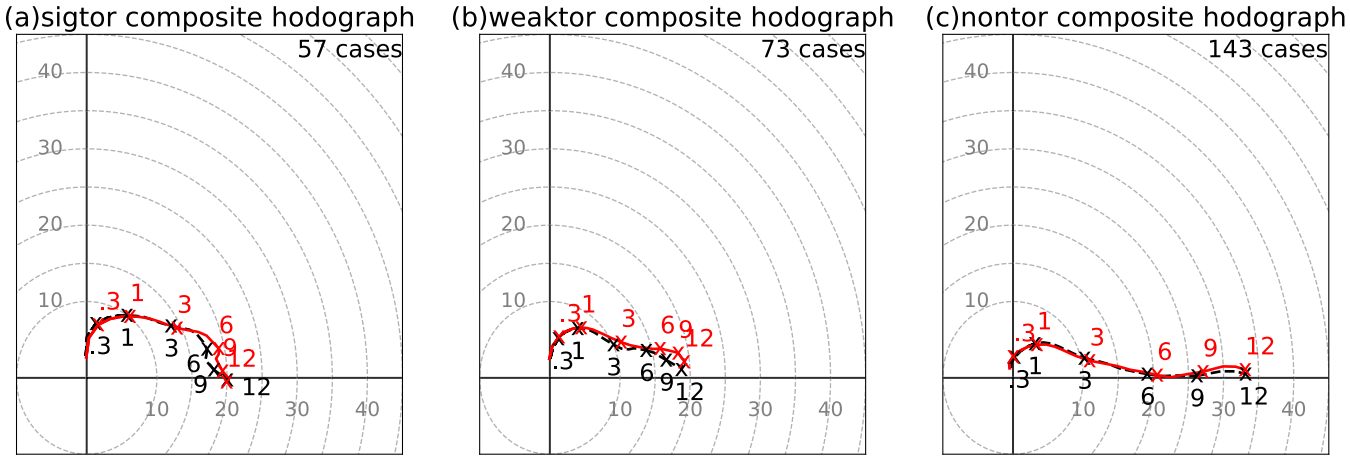

FIGURE 6 Composite hodographs are presented for (a) significantly tornadic supercells (sig-tor; 57 cases), (b) weakly tornadic supercells (weak-tor; 73 cases), and (c) non-tornadic supercells (non-tor; 144 cases) before (dashed black) and after (solid red) realignment of the 0–6-km shear vector. The curves are labeled with heights above ground level (AGL) in kilometers. The wind speed unit is $m \cdot s^{-1}$. [Colour figure can be viewed at wileyonlinelibrary.com]

3.3 | Improvements to the STP in China

3.3.1 | The current STP

The STP effectively distinguishes between tornadic and non-tornadic supercells in the United States. A higher STP indicates a greater likelihood of tornado occurrence. In this section, we first examine whether STP, represented by two expressions in Equations (1) and (2), can also have good predictive skills for tornadic versus non-tornadic supercells in China. As shown in Figure 7a, the STPfix median of non-tornadic supercells calculated based on Equation (1) is equal to that of weakly tornadic supercells, and no substantial differences are observed in their STPfix distributions. The 25th percentile of STPfix for significantly tornadic supercells cannot match the 75th percentile of STPfix for non-tornadic supercells (Figure 7a). The TSS value of STPfix is 0.29 (Table 2). Therefore, the STPfix as given in Equation (1) may not be well suited for China. The performance of STPeff is even worse. The distribution of STPeff for non-tornadic cases is obviously higher than that for weakly tornadic supercells (Figure 7b). STPeff gets a TSS value of 0.14 (Table 2). Clearly, the TSS values of STPfix and STPeff based on Equations (1) and (2) are much lower in China compared to those in the United States, where they are usually higher than 0.45 (Thompson *et al.*, 2003, 2011). The TSS score for STPfix for China overall is lower due to the significantly low score of 0.08 in the CNS region (Table 3) while that in the CNC region is relatively high at 0.51. A similar pattern is observed for STPeff, and another notable low TSS value of 0.06 is found in the CNN region (Table 3).

From Figure 7a,b, along with the TSS values of STP, we can conclude that the STP parameters as defined in Equations (1) and (2) are not effective in discriminating tornadic supercells, especially weakly tornadic supercells, from non-tornadic supercells in China. Further insights into why STP performs poorly can be gleaned from the values of each component of STP across different storm types (Figure 8a,b). The thermodynamic components of STPfix calculated for the SB parcels among different storm types show similar distributions (Figure 8a). The values of the CAPE term have a slight downward trend from tornadic to non-tornadic supercells (Figure 8a). The values of the LCL term on the box-and-whisker are all one (maximum for the LCL term) for tornadic supercells and are below one from the 10th to the 25th percentile for non-tornadic supercells (Figure 8a). Using the SRH term instead of thermodynamic terms improves the performance of discerning tornadoes, as 75% of the significantly tornadic supercells have SRH term values greater than the SRH term median for non-tornadic supercells (Figure 8a). However, the distributions of the SRH term are similar between weakly tornadic and non-tornadic supercells (Figure 8a). The shear term of STPfix performs even worse than thermodynamic terms. The majority of shear-term values for non-tornadic supercells are higher than those for tornadic supercells (Figure 8a), attributed to the characteristics of SHR6 in China supercell cases.

The CAPE term of STPeff shows a similar distribution among three storm types (Figure 8b). About half of the cases for each storm type have LCL term values equal to one (Figure 8b). The values of the CIN term are equal to the maximum of one for most cases (Figure 8b). Similar

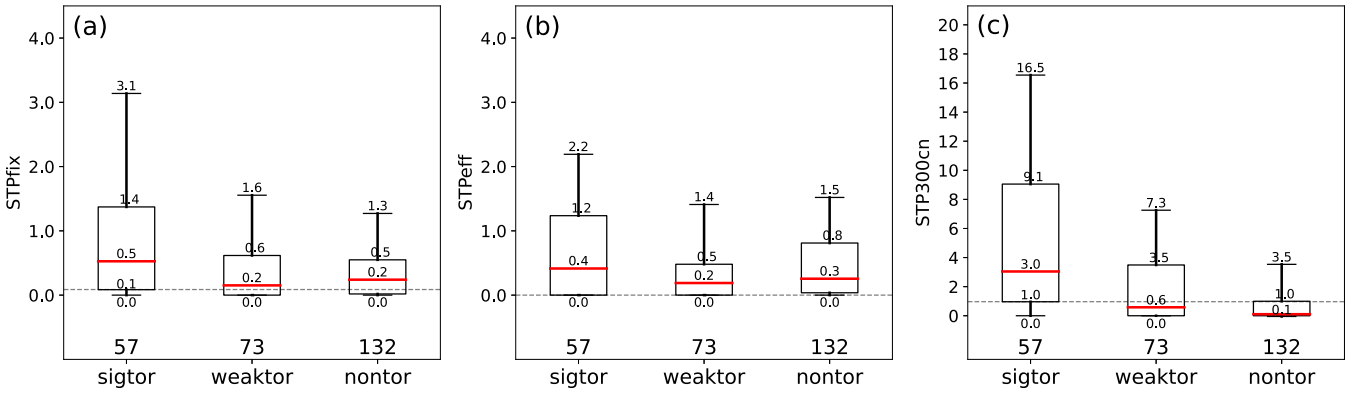

FIGURE 7 Box-and-whisker plots of (a) STPfix, (b) STPeff, and (c) STP300cn for significantly tornadic supercells (sig-tor), weakly tornadic supercells (weak-tor), and non-tornadic supercells (non-tor). The gray dashed line represents the 25th percentile of the sig-tor box for each STP. Other descriptions are as in Figure 3. [Colour figure can be viewed at wileyonlinelibrary.com]

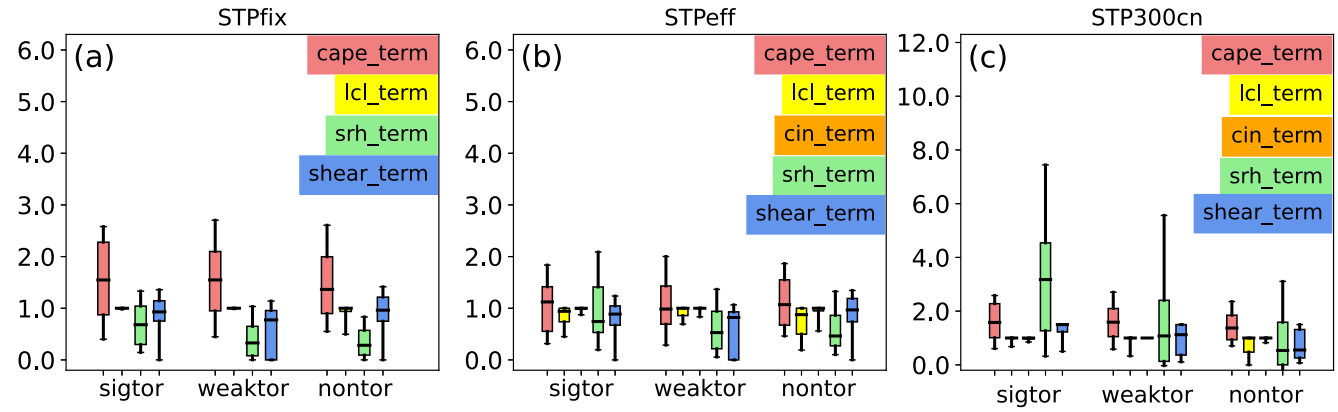

FIGURE 8 Box-and-whisker plots of each term in (a) STPfix, (b) STPeff, and (c) STP300cn for significantly tornadic supercells (sig-tor), weakly tornadic supercells (weak-tor), and non-tornadic supercells (non-tor). Other descriptions are as in Figure 3. [Colour figure can be viewed at wileyonlinelibrary.com]

to the SRH term of STPfix, the SRH term of STPeff fails to differentiate between weakly tornadic and non-tornadic supercells (Figure 8b). The shear term of STPeff resembles that of STPfix (Figure 8b).

3.3.2 | Calibrating STP for China

Due to the limited skill of the original formulations of STP parameters in forecasting tornadoes in China, the thermodynamic and kinematic terms in STP are calibrated based on their characteristics. When evaluating the performance of CAPE and LCL for different types of lifted parcels, the SB and MU parcels tend to exhibit better predictive skills compared to the ML parcel type. In fact, the differences between SB-based and MU-based parameters are minimal, as most of the cases used in this paper are surface-based. In this case, we choose to use CAPE, LCL, and CIN based on MU parcels in the revised STP formulation, as they are more effective for elevated storms.

As previously shown, the use of shallow-layer SRH and shallow-layer wind shear results in better performance. Replacing the deep-layer SRH and shear with shallow-layer SRH and shear in STP could potentially improve tornado forecasting in China. We examine the TSS values of SRH and wind shear when the top of the SRH integration and the shear layer increases from 200 to 6000 m AGL, respectively (Figure 9). Our results demonstrate an increasing trend of TSS as the layer top height decreases for both SRH and shear. Consistent with previous studies (Coffer *et al.*, 2019, 2020), the shallow layer of SRH indeed has a higher TSS value. Among the tested shallow-layer depths of SRH, SRH over 0–300 m depth or SRH300 exhibits the best forecasting skill. Similarly, the 0–300 m shear, SHR300, also has the highest skill among tested wind shears over various depths. The kinematic

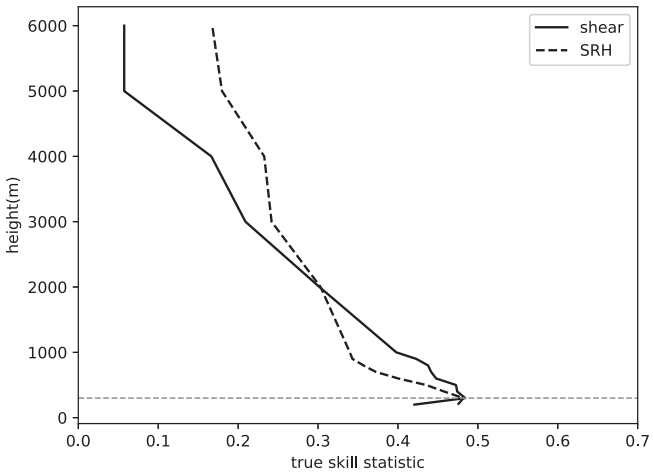

FIGURE 9 True skill statistic (TSS) at the optimal threshold for various depths of storm-relative helicity (SRH) (dashed line) and shear (solid line) integrated from 200 to 6000 m (i.e., 200, 300, 400, 500, 600, 700, 800, 900,1000, 2000, 3000, 4000, 5000, and 6000 m) above ground level (AGL) for discriminating between significantly tornadic and non-tornadic supercells. The dashed gray line denotes the corresponding layer of the max TSS for SRH and shear. TSS is calculated at 1000 evenly spaced thresholds of the entire ERA5 sounding dataset for each layer of SRH and shear.

components of STP are therefore replaced with parameters based on the fixed 0–300-m depth.

To further enhance the predictive skill of the revised STP for tornadoes in China, we made several adjustments to the STP formulation. Firstly, as indicated earlier, we used MU-based thermodynamic parameters and kinematic parameters over a fixed depth of 300 m. Additionally, to preserve the threshold of 1 for STP, the normalization denominators of some terms are adjusted. It is worth noting that modifying the denominator will not affect the maximum TSS value of each term in STP, but it does impact the optimal threshold for each term. With these changes, the formulation of the calibrated STP, which we call STP300cn, is given by.

$$\mathrm{STP300cn} = \left(\frac{\mathrm{MUCAPE}}{2000\ \mathrm{J\cdot kg^{-1}}}\right) \times \left(\frac{\mathrm{MUCIN}+200}{150\ \mathrm{J\cdot kg^{-1}}}\right) \times \left(\frac{1600-\mathrm{MULCL}}{600\ \mathrm{m}}\right) \times \left(\frac{\mathrm{SRH300}}{12\ \mathrm{m^2\cdot s^{-2}}}\right) \times \left(\frac{\mathrm{SHR300}}{1.9\ \mathrm{m\cdot s^{-1}}}\right). \quad (4)$$

Here are the calculation rules we apply to different terms in STP300cn. Same as the original STP, the MUCIN term is 0.0 when MUCIN is less than $-150\,\mathrm{J\cdot kg^{-1}}$ and is 1.0 when MUCIN exceeds $-50\,\mathrm{J\cdot kg^{-1}}$. Given the MULCL and SHR300 distributions for supercells in China, we make adjustments to the MULCL and SHR terms. The MULCL term is set to 0 when MULCL is greater than 1600 m and is set to 1 when MULCL is less than 1000 m. The SHR300 term equals 1.5 when SHR300 is greater than $2.85\,\mathrm{m\cdot s^{-1}}$ and there is no lower bound. Besides, the MUCAPE and SRH300 terms still have no upper bounds and their normalizing denominators have been changed to $2000\,\mathrm{J\cdot kg^{-1}}$ and $12\ \mathrm{m^2\cdot s^{-2}}$, respectively.

With the above calibrations, the TSS value of STP300cn is increased to 0.51 for the China cases, which is more than twice those of the original STPfix and STPeff (Table 2). Compared with the original STPs, STP300cn can distinguish much better between significantly tornadic and non-tornadic supercells in China, which is evident from the box-and-whisker plot in Figure 7. The forecasting ability of STP300cn is further evidenced by comparing the position of the gray dashed line representing the 25th percentile value of STP for significantly tornadic supercells across all subfigures in Figure 7. Unlike the 25th percentile values of STPfix and STPeff, which are similar for significantly tornadic and non-tornadic supercells (Figure 7a,b), the 25th percentile of STP300cn for significantly tornadic supercells matches the 75th percentile for non-tornadic ones (Figure 7c). STP300cn also exhibits a markedly higher distribution for weakly tornadic supercells than for non-tornadic supercells (Figure 7c).

The performance of STP300cn also varies across the three subregions in China. According to Table 3, STP300cn in CNC has the highest forecast skill with a TSS value of 0.66. This is primarily due to the impressive skills of SRH300, SHR300, and LCL in CNC. Meanwhile, STP300cn in both CNN and CNS regions achieve lower values (~0.4; Table 3) compared to the CNC region. As discussed in Section 3.1, significant tornadoes in the CNN region are primarily driven by favorable kinematic conditions rather than favorable thermodynamic conditions. The lower TSS values of thermodynamic parameters result in a relatively low TSS value of STP300cn compared to that in the CNC region. Therefore, when predicting significant tornadoes in the CNN region, attention should also be paid to the individual kinematic parameters in addition to STP300cn. In the CNS region, the abundant moisture, along with relatively weak wind shear and lower horizontal streamwise vorticity, contributes to the lower TSS values of LCL and the kinematic terms in STP300cn. Still, in the CNN and CNS regions, the performance of STP300cn is much superior to those of the original STP parameters.

STP300cn also performs better than the original STPs in distinguishing between weakly tornadic and non-tornadic supercells in each region (Table S1 in the Supplementary Information), and the overall performance characteristics of the parameters across three regions are similar to those in distinguishing significantly tornadic and non-tornadic supercells.

Although the superior performance of kinematic parameters over thermodynamic parameters has been discussed in Section 3, the performance of each component in STP300cn is examined further in this subsection. With a TSS value of 0.05 (Table 2), MUCIN exhibits the poorest performance among the thermodynamic components in STP300cn. On the other hand, the forecasting skills of MUCAPE and MULCL show improvement compared to MUCIN ($TSS_{MUCAPE} = 0.18$, $TSS_{MULCL} = 0.29$; Table 2). The median of MUCAPE for significantly tornadic cases increases by about 11% compared to that for non-tornadic cases (Figure 3d). Additionally, the MULCL median increases by nearly 31% from significantly tornadic cases to non-tornadic cases (Figure 3e). However, the distributions of the CAPE and LCL terms among the three types of supercells are still highly overlapped (Figure 8c). Therefore, the thermodynamic parameters in STP300cn still do not perform well by themselves, and their low skills in CNN contribute negatively to the overall score over China.

With an optimal threshold of 10.4 $m^2 \cdot s^{-2}$, SRH300 has a higher TSS value of 0.48 compared to SRH1 of 0.34 or ESRH of 0.29 (Table 2). Similarly, SHR300 has a much higher TSS value of 0.48 compared to SHR6 of 0.06 or EBWD of 0.01 (Table 2). Not surprisingly, the kinematic terms in STP300cn exhibit better performance when compared to the kinematic terms in the original STP. Especially, the 25th percentile of the SRH300 term for significantly tornadic cases closely matches the median SRH300 term for weakly tornadic cases and the 75th percentile of the SRH300 term for non-tornadic cases (Figure 8c).

Figure 10 is a performance diagram that displays additional skill metrics, including success ratio (1 − FAR), POD, bias *B*, and critical success index (CSI), for each term in STP300cn (Roebber, 2009). The kinematic terms at the optimal TSS values perform better, with CSI values of about 0.45. However, they show a tendency to over-forecast, as indicated by the high biases, particularly for SRH300. MUCAPE at the optimal TSS shows nearly no bias but a much lower CSI value of ~0.25. In contrast, MUCIN at the optimal TSS has significant over-forecast, corresponding to a high POD value and a low success ratio. MULCL achieves the highest CSI values among thermodynamic terms, although it is also somewhat over-forecasted.

4 | DISCUSSION

In addition to assessing STP, we also investigated the efficacy of other combined parameters. BRN $\left[\mathrm{BRN} = \mathrm{MLCAPE}/0.5\left(u_{\mathrm{avg}}\right)^2\right]$ has served as a predictor for supercells since it was initially explored through numerical simulations (Weisman & Klemp, 1982). Environments with BRN less than 50 are conducive to supercell formation, while environments with BRN above 50 favor multicellular events. With a similar BRN mean value for significantly tornadic and non-tornadic supercells (Figure 4), BRN achieves the lowest TSS value of 0.07 (Table 2) among combined parameters. Another combined parameter, EHI, is developed to better determine the potential for supercells and tornadoes in a given environment (Hart & Korotky, 1991). The TSS value for 0–1-km EHI [EHI = (CAPE)(SRH1/160000)] is the same as that for STPfix, which is 0.26 (Table 2). Generally, most strong tornadoes occur with EHI values of 3.0–3.9 (Davies, 1993), but the mean values of EHI for significantly tornadic cases is 0.7 and for non-tornadic cases is 0.4 in China (Figure 4). VGP = $\left[S(\mathrm{CAPE})^{1/2}\right]$, where *S* represents the 0–4-km mean shear, and is derived from the physical concept of tilting of vorticity (Rasmussen & Blanchard, 1998). Similarly, VGP has a low TSS value of 0.17 (Table 2). SCP [SCP = (MUCAPE/1000 J · kg^{-1})(ESRH/50 $\mathrm{m}^2 \cdot \mathrm{s}^{-2}$)(EBWD/20 $\mathrm{m} \cdot \mathrm{s}^{-1}$)], which has been formulated to identify environments that support supercells (Thompson *et al.*, 2003), also has a low TSS value of 0.18 (Table 2).

To sum up, the TSS values of the combined parameters above are all less than 0.3. This is not surprising, as they are combinations of CAPE and deep-layer shear. CAPE and deep-layer shear may not correlate directly with the formation of the low-level mesocyclone (Brooks *et al.*, 1994). In contrast, the shallow-layer shear and SRH, as well as other useful thermodynamic parameters, should be paid closer attention in China.

The TSS value of STP300cn ($TSS_{STP300cn} = 0.51$; Table 2) is only slightly higher than the TSS values for individual kinematic parameters ($TSS_{SRH300} = TSS_{SHR300} = 0.48$; Table 2), indicating that thermodynamic terms in STP300cn only make small contributions. Future research should focus on identifying and incorporating more effective thermodynamic parameters such as entraining CAPE (Bai et al., 2020; Sueki & Niino, 2016) into combined parameters. This entails a comprehensive exploration of various atmospheric thermodynamic properties to ascertain their significance in enhancing the predictive capability of combined parameters for distinguishing between tornadic and non-tornadic supercells.

Coffer *et al.* (2020) obtained a significant enhancement in the discrimination between tornadic and non-tornadic supercells through the utilization of the 0–100-m AGL layer SRH. This suggests that the layer with the best predictive skill for SRH or shear in China may need further exploration. Higher vertical resolution observations and model output data are needed to further assess the performance of shallow-layer SRH and shear for supercell environments in China, which should

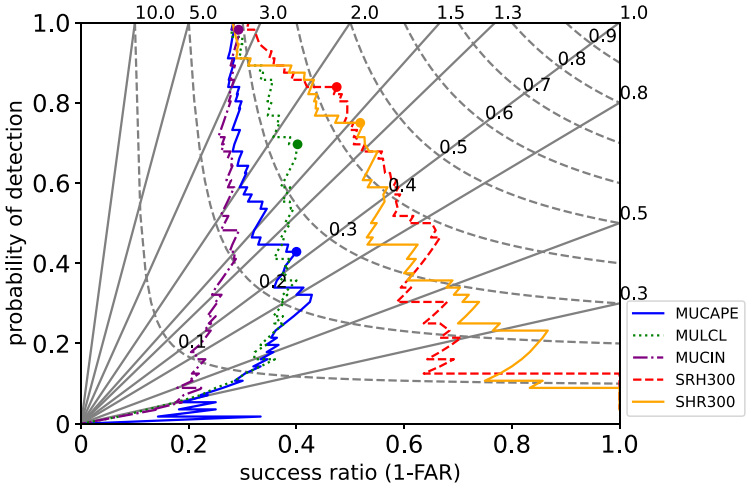

FIGURE 10 Performance diagram summarizing the success ratio (1 – FAR [false alarm ratio]), probability of detection, bias, and critical success index at 1000 evenly distributed thresholds of the entire ERA5 sounding dataset for each term in STP300cn, which includes the MUCAPE, MULCL, MUCIN, SRH300, and SHR300 terms. Each curve starts with a probability of detection of 1, and as the threshold increases, it shows a decrease in probability of detection. The dot on each curve indicates the threshold with the optimal TSS value. Bias scores are shown as sloping solid lines with labels on the outward extension, and the labeled dashed contours are critical success index (CSI). The diagonal straight line indicates no bias and the top right corner indicates perfect CSI. [Colour figure can be viewed at wileyonlinelibrary.com]

be helpful for obtaining more reliable and insightful conclusions.

This paper primarily focuses on the environmental characteristics that distinguish tornadic supercells from non-tornadic supercells in China. Future research could utilize soundings from both tornadic and non-tornadic supercells in China to conduct idealized simulations aimed at investigating how processes beyond environmental factors contribute to tornado formation. Such studies could help identify additional influences, such as storm dynamics or mesoscale interactions, that may play critical roles in tornado genesis, providing a more comprehensive understanding of the factors involved in tornado occurrence.

5 | SUMMARY AND CONCLUSIONS

In this paper, we seek to compare the environmental characteristics of tornadic and non-tornadic supercells in China. The ERA5 dataset that has higher spatial and temporal resolutions compared to other global reanalysis datasets is used to extract proximity soundings and calculate environmental parameters. A sample of 130 tornadic supercells and 143 non-tornadic supercells from 2002 to 2021 is used. Supercells are categorized as significantly tornadic (sig-tor, those rated EF2–EF4), weakly tornadic (weak-tor, those rated EF1) and non-tornadic (non-tor). Tornadic supercells are primarily concentrated in the eastern regions of China, while non-tornadic supercells are more widely distributed. In addition to their prevalence in eastern China, non-tornadic supercells also extend into central regions. Tornadic supercells have a similar diurnal distribution to non-tornadic supercells. However, with tornadic supercells peaking in July and non-tornadic supercells peaking in April, their seasonal distributions are different. To explore the regional characteristics, China is divided into northern China (CNN), central China (CNC), and southern China (CNS). TSS is used to identify the environmental parameters that are effective in distinguishing between significantly tornadic and non-tornadic supercells.

Firstly, we examined thermodynamic parameters including CAPE, LCL, and CIN, based on ML, SB, and MU lifted parcels. Additionally, kinematic parameters including SRH300, SRH1, ESRH, SHR300, EBWD, and SHR6 were analyzed. With the median of CAPE for significantly tornadic supercells being either less than or similar to that for weakly tornadic supercells, and only slightly greater than that for non-tornadic supercells, CAPE exhibits limited forecasting skill (TSS less than 0.2). CAPE based on SB or MU parcels performs better. Weakly tornadic supercells have the lowest LCL median and non-tornadic supercells have the highest LCL median. TSS values of LCL are less than 0.3. CIN (with TSS similar to 0.1) shows even worse performance than CAPE and LCL. The low performance of these thermodynamic parameters in China is partly related to the limited skill in the CNN region and the worse performance of LCL in the CNS region. Thermodynamic parameters in CNC perform better. We also examined other thermodynamic parameters like lowRH, LR85, LR75 and LFC. There are no large distinctions of these parameters across various storm types.

SHR6 and EBWD of non-tornadic supercells are higher than those of weakly tornadic supercells, and TSS values of SHR6 and EBWD are both less than 0.1. SRH300 and SHR300 show the best forecast skill among SRH and shear evaluated over other depths. The TSS values of SRH300 and SHR300 perform best in the CNC region (~0.6) while also exhibiting a notable score of approximately 0.5 in the CNN region. However, in the CNS region, both parameters show relatively low TSS values (SRH ~ 0.3 and SHR ~ 0.4). Moreover, SRH300 and SHR300 of weakly

tornadic supercells are obviously higher than those of non-tornadic supercells.

Further, we examined whether the original STP parameters (STPfix and STPeff) can effectively discriminate tornadic supercells from non-tornadic supercells in China. The results reveal that both STPfix and STPeff based on the original formulations that were calibrated for the U.S. cases have limited skill ($TSS_{STPfix} = 0.29$ and $TSS_{STPeff} = 0.14$) for the China cases, and their distributions fail to effectively distinguish weakly tornadic from non-tornadic supercells. To improve the performance, we composed a new STP formulation by using MUCAPE, MULCL, MUCIN, SRH300, and SHR300, to obtain a parameter we call STP300cn. The TSS value of STP300cn is 0.51, significantly higher than those of STP_{fix} and STP_{eff}. Regional differences also exist in STP300cn. It exhibits a great performance in CNC (TSS = 0.66), CNS (TSS = 0.42) and a TSS value of 0.37 in CNN, which are all much higher than TSS values achieved by the original STPs. Moreover, the performance of each term in STP300cn is compared in this paper. Kinematic terms (SRH300 and SHR300) outperform thermodynamic terms (MUCAPE, MULCL, and MUCIN), though they tend to be slightly over-forecasted. Among thermodynamic terms, MUCIN has the worst forecast skill.

This study is limited by the relatively small sample size of tornadic and non-tornadic supercell cases in China, as well as notable differences in their spatial and temporal distributions. Additionally, there may be potential inaccuracies in the extracted environmental soundings from the ERA5 dataset. Further studies should try to include additional cases and use more accurate regional reanalysis or incorporate observed soundings when they are available.

ACKNOWLEDGEMENTS

This work was primarily supported by NSFC grant 41730965.

FUNDING INFORMATION

NSFC grant 41730965.

DATA AVAILABILITY STATEMENT

The ERA5 reanalysis dataset can be downloaded online (https://cds.climate.copernicus.eu/). The software used in this paper is available online (https://github.com/sharppy/SHARPpy). The list of tornadic and non-tornadic supercells used in this paper and the related codes can be accessed at https://doi.org/10.7910/DVN/OH0VKD.

ORCID

Ruqian Zhang https://orcid.org/0009-0003-9746-6519
Ming Xue https://orcid.org/0000-0003-1976-3238

REFERENCES

Bai, L., Meng, Z., Sueki, K., Chen, G. & Zhou, R. (2020) Climatology of tropical cyclone tornadoes in China from 2006 to 2018. *Science China Earth Sciences*, 63, 37–51. Available from: https://doi.org/10.1007/s11430-019-9391-1

Beebe, R.G. (1958) Tornado proximity soundings. *Bulletin of the American Meteorological Society*, 39, 195–201. Available from: https://doi.org/10.1175/1520-0477-39.4.195

Blumberg, W.G., Halbert, K.T., Supinie, T.A., Marsh, P.T., Thompson, R.L. & Hart, J.A. (2017) SHARPpy: an open-source sounding analysis toolkit for the atmospheric sciences. *Bulletin of the American Meteorological Society*, 98, 1625–1636. Available from: https://doi.org/10.1175/BAMS-D-15-00309.1

Brooks, H.E., Doswell, C.A., III & Cooper, J. (1994) On the environments of tornadic and nontornadic mesocyclones. *Weather and Forecasting*, 9, 606–618.

Brooks, H.E., Lee, J.W. & Craven, J.P. (2003) The spatial distribution of severe thunderstorm and tornado environments from global reanalysis data. *Atmospheric Research*, 67–68, 73–94. Available from: https://doi.org/10.1016/S0169-8095(03)00045-0

China Meteorological Administration. (2005–2022) *Yearbook of meteorological disasters in China (in Chinese)*. Beijing, China: Meteorological Press.

Coffer, B. & Parker, M.D. (2015) Impacts of increasing low-level shear on supercells during the early evening transition. *Monthly Weather Review*, 143, 1945–1969. Available from: https://doi.org/10.1175/MWR-D-14-00328.1

Coffer, B. & Parker, M.D. (2017) Simulated supercells in nontornadic and tornadic VORTEX2 environments. *Monthly Weather Review*, 145, 149–180. Available from: https://doi.org/10.1175/MWR-D-16-0226.1

Coffer, B. & Parker, M.D. (2018) Is there a "tipping point" between simulated nontornadic and tornadic supercells in VORTEX2 environments? *Monthly Weather Review*, 146, 2667–2693. Available from: https://doi.org/10.1175/MWR-D-18-0050.1

Coffer, B., Parker, M.D., Dahl, J.M.L., Wicker, L.J. & Clark, A.J. (2017) Volatility of tornadogenesis: an ensemble of simulated nontornadic and tornadic supercells in VORTEX2 environments. *Monthly Weather Review*, 145, 4605–4625. Available from: https://doi.org/10.1175/MWR-D-17-0152.1

Coffer, B., Parker, M.D., Thompson, R.L., Smith, B.T. & Jewell, R.E. (2019) Using near-ground storm relative helicity in supercell tornado forecasting. *Weather and Forecasting*, 34, 1417–1435. Available from: https://doi.org/10.1175/WAF-D-19-0115.1

Coffer, B., Taszarek, M. & Parker, M.D. (2020) Near-ground wind profiles of tornadic and nontornadic environments in the United States and Europe from ERA5 reanalyses. *Weather and Forecasting*, 35, 2621–2638. Available from: https://doi.org/10.1175/WAF-D-20-0153.1

Craven, J.P. & Brooks, H.E. (2004) Baseline climatology of sounding derived parameters associated with deep, moist convection. *National Weather Digest*, 28, 13–24.

Davies, J.M. (1993) Hourly helicity, instability, and EHI in forecasting supercell tornadoes. In: *17th Conference on Severe Local Storms*. Kansas City, MO: American Meteorological Society, pp. 107–111.

Davies, J.M. (2004) Estimations of CIN and LFC associated with tornadic and nontornadic supercells. *Weather and Forecasting*, 19, 714–726. Available from: https://doi.org/10.1175/1520-0434(2004)019<0714:EOCALA>2.0.CO;2

Davies-Jones, R. (1984) Streamwise vorticity: the origin of updraft rotation in supercell storms. *Journal of the Atmospheric Sciences*, 41, 2991–3006.

Davies-Jones, R. (2015) A review of supercell and tornado dynamics. *Atmospheric Research*, 158, 274–291. Available from: https://doi.org/10.1016/j.atmosres.2014.04.007

Davies-Jones, R.P., Burgess, D. & Foster, M. (1990) Test of helicity as a forecast parameter. In: *16th Conference on Severe Local Storms*. Kananaskis Park, AB, Canada: American Meteorological Society, pp. 588–592.

Ding, Y. (2008) *The collection of meteorological disasters Records in China* (in Chinese). Beijing, China: Meteorological Press, p. 948.

Donaldson, R.J. & Desrochers, P.R. (1990) Improvement of tornado warnings by doppler radar measurement of mesocyclone rotational kinetic energy. *Weather and Forecasting*, 5, 247–258.

Doswell, C.A., Davies-Jones, R. & Keller, D.L. (1990) On summary measures of skill in rare event forecasting based on contingency tables. *Weather and Forecasting*, 5, 576–585.

Doswell, C.A. & Evans, J.S. (2003) Proximity sounding analysis for derechos and supercells: an assessment of similarities and differences. *Atmospheric Research*, 67-68, 117–133. Available from: https://doi.org/10.1016/S0169-8095(03)00047-4

Doswell, C.A. & Flueck, J.A. (1989) Forecasting and verifying in a field research project: DOPLIGHT'87. *Weather and Forecasting*, 4, 97–109.

Edwards, R., Dean, A.R., Thompson, R.L. & Smith, B.T. (2012) Convective modes for significant severe thunderstorms in the contiguous United States. Part III: tropical cyclone tornadoes. *Weather and Forecasting*, 27, 1507–1519. Available from: https://doi.org/10.1175/WAF-D-11-00117.1

Evans, J.S. & Doswell, C.A. (2001) Examination of derecho environments using proximity soundings. *Weather and Forecasting*, 16, 329–342. Available from: https://doi.org/10.1175/1520-0434(2001)016<0329:EODEUP>2.0.CO;2

Fan, W. & Yu, X. (2015) Characteristics of spatial-temporal distribution of tornadoes in China (in Chinese with English abstract). *Meteorological Monthly*, 41, 793–805. Available from: https://doi.org/10.7519/j.issn.1000-0526.2015.07.0012015

Fawbush, E.J. & Miller, R.C. (1954) The types of air masses in which north American tornadoes form. *Bulletin of the American Meteorological Society*, 35, 154–165. Available from: https://doi.org/10.1175/1520-0477-35.4.154

Fischer, J. & Dahl, J.M.L. (2022) Transition of near-ground vorticity dynamics during tornadogenesis. *Journal of the Atmospheric Sciences*, 79, 467–483. Available from: https://doi.org/10.1175/JAS-D-21-0181.1

Hart, J.A. & Korotky, W. (1991) *The SHARP workstation v 1.50 users guide*. Bohemia, NY: NOAA/NWS Document, p. 30.

Hersbach, H., Bell, B., Berrisford, P., Hirahara, S., Horányi, A., Muñoz-Sabater, J. et al. (2020) The ERA5 global reanalysis. *Quarterly Journal of the Royal Meteorological Society*, 146, 1999–2049. Available from: https://doi.org/10.1002/qj.3803

Klees, A.M., Richardson, Y.P., Markowski, P.M., Weiss, C., Wurman, J. & Kosiba, K.K. (2016) Comparison of the tornadic and nontornadic supercells intercepted by VORTEX2 on 10 June 2010. *Monthly Weather Review*, 144, 3201–3231. Available from: https://doi.org/10.1175/MWR-D-15-0345.1

Lemon, L.R. & Doswell, C.A. (1979) Severe thunderstorm evolution and mesocyclone structure as related to tornadogenesis. *Monthly Weather Review*, 107, 1184–1197.

Markowski, P., Hannon, C., Frame, J., Lancaster, E., Pietrycha, A., Edwards, R. et al. (2003) Characteristics of vertical wind profiles near supercells obtained from the rapid update cycle. *Weather and Forecasting*, 18, 1262–1272. Available from: https://doi.org/10.1175/1520-0434(2003)018<1262:COVWPN>2.0.CO;2

Markowski, P.M. & Richardson, Y. (2014) The influence of environmental low-level shear and cold pools on tornadogenesis: insights from idealized simulations. *Journal of the Atmospheric Sciences*, 71, 243–275. Available from: https://doi.org/10.1175/JAS-D-13-0159.1

Markowski, P.M., Straka, J.M. & Rasmussen, E.N. (1998) A preliminary investigation of the importance of helicity location in the hodograph. In: *19th conference on severe local storms*. Minneapolis, MN: American Meteorological Society, pp. 230–233.

Markowski, P.M., Straka, J.M. & Rasmussen, E.N. (2002) Direct surface thermodynamic observations within the rear-flank downdrafts of nontornadic and tornadic supercells. *Monthly Weather Review*, 130, 1692–1721. Available from: https://doi.org/10.1175/1520-0493(2002)130<1692:DSTOWT>2.0.CO;2

Mead, C. (1997) The discrimination between tornadic and nontornadic supercell environments: a forecasting challenge in the southern United States. *Weather and Forecasting*, 12, 379–387.

Peirce, C.S. (1884) The numerical measure of the success of predictions. *Science*, 4, 453–454. Available from: https://doi.org/10.1126/science.ns-4.93.453-a

Rasmussen, E.N. & Wilhelmson, R.B. (1983) Relationships between storm characteristics and 1200 GMT hodographs, low-level shear, and stability. In: *13th Conference on Severe Local Storms*. Tulsa, OK: American Meteorological Society, pp. J5–J8.

Rasmussen, E.N. & Blanchard, D.O. (1998) A baseline climatology of sounding-derived supercell and tornado forecast parameters. *Weather and Forecasting*, 13, 1148–1164.

Roebber, P.J. (2009) Visualizing multiple measures of forecast quality. *Weather and Forecasting*, 24, 601–608. Available from: https://doi.org/10.1175/2008WAF2222159.1

Rotunno, R., Markowski, P.M. & Bryan, G.H. (2017) "Near ground" vertical vorticity in supercell thunderstorm models. *Journal of the Atmospheric Sciences*, 74, 1757–1766. Available from: https://doi.org/10.1175/JAS-D-16-0288.1

Schenkman, A.D., Xue, M. & Hu, M. (2014) Tornadogenesis in a high-resolution simulation of the 8 may 2003 Oklahoma City supercell. *Journal of the Atmospheric Sciences*, 71, 130–154. Available from: https://doi.org/10.1175/JAS-D-13-073.1

Showalter, A.K. & Fulks, J.R. (1943) *Preliminary report on tornadoes*. Washington: U.S. Weather Bureau, p. 162.

Stensrud, D.J., Cortinas, J. & Brooks, H.E. (1997) Discriminating between tornadic and nontornadic thunderstorms using mesoscale model output. *Weather and Forecasting*, 12, 613–632.

Sueki, K. & Niino, H. (2016) Toward better assessment of tornado potential in typhoons: Significance of considering entrainment effects for CAPE. *Geophysical Research Letters*, 43, 12597–12604. Available from: https://doi.org/10.1002/2016GL070349

Taszarek, M., Allen, J.T., Púčik, T., Hoogewind, K.A. & Brooks, H.E. (2020) Severe convective storms across Europe and the United States. Part II: ERA5 environments associated with lightning, large hail, severe wind, and tornadoes. *Journal of Climate*, 33, 10263–10286. Available from: https://doi.org/10.1175/JCLI-D-20-0346.1

Thompson, R.L. (1998) Eta model storm-relative winds associated with tornadic and nontornadic supercells. *Weather and Forecasting*, 13, 125–137.

Thompson, R.L., Edwards, R., Hart, J.A., Elmore, K.L. & Markowski, P.M. (2003) Close proximity soundings within supercell environments obtained from the rapid update cycle. *Weather and Forecasting*, 18, 1243–1261. Available from: https://doi.org/10.1175/1520-0434(2003)018<1243:CPSWSE>2.0.CO;2

Thompson, R.L., Edwards, R. & Mead, C.M. (2011) An update to the supercell composite and significant tornado parameters. In: *22nd Conference on Severe Local Storms*. Norman, OK: American Meteorological Society.

Thompson, R.L., Mead, C.M. & Edwards, R. (2007) Effective storm-relative helicity and bulk shear in supercell thunderstorm environments. *Weather and Forecasting*, 22(1), 102–115. Available from: https://doi.org/10.1175/WAF969.1

Trapp, R.J. (1999) Observations of nontornadic low-level mesocyclones and attendant tornadogenesis failure during VORTEX. *Monthly Weather Review*, 127, 1693–1705.

Veloso-Aguila, D., Rasmussen, K.L. & Maloney, E.D. (2023) Tornadoes in southeast south America: mesoscale to planetary-scale environments. *Monthly Weather Review*, 152, 295–318. Available from: https://doi.org/10.1175/MWR-D-22-0248.1

Wakimoto, R.M. & Cai, H. (2000) Analysis of a nontornadic storm during VORTEX 95. *Monthly Weather Review*, 128, 565–592. Available from: https://doi.org/10.1175/1520-0493(2000)128,0565:AOANSD.2.0.CO;2

Wakimoto, R.M., Cai, H. & Murphey, H.V. (2004) The superior, Nebraska, supercell during BAMEX. *Bulletin of the American Meteorological Society*, 85, 1095–1106. Available from: https://doi.org/10.1175/BAMS-85-8-1095

Wang, X., Yu, X. & Zhou, X. (2015) Study of Northeast China tornadoes: the environmental characteristics (in Chinese with English abstract). *Acta Meteorologica Sinica*, 73, 425–441.

Weisman, M.L. (1996) On the use of vertical wind shear versus helicity in interpreting supercell dynamics. In: *18th Conference on Severe Local Storms*. San Francisco, CA: American Meteorological Society, pp. 200–204.

Weisman, M.L. & Klemp, J.B. (1982) The dependence of numerically simulated convective storms on vertical wind shear and buoyancy. *Monthly Weather Review*, 110, 504–520.

Weisman, M.L. & Klemp, J.B. (1984) The structure and classification of numerically simulated convective storms in directionally varying wind shears. *Monthly Weather Review*, 112, 2479–2498.

Weisman, M.L. & Klemp, J.B. (1986) Characteristics of isolated convective storms. In: *Mesoscale meteorology and forecasting*. Boston, MA: American Meteorological Society, pp. 331–358. Available from: https://doi.org/10.1007/978-1-935704-20-1_15

Wilks, D.S. (2020) *Statistical Methods in the Atmospheric Sciences*, 4rd edition. Oxford, UK: Elsevier, p. 381.

Yu, X., Zhao, J. & Fan, W. (2021) Tornadoes in China: spatiotemporal distribution and environmental characteristics (in Chinese with English abstract). *Journal of Tropical Meteorology*, 37, 681–692. Available from: https://doi.org/10.16032/j.issn.1004-4965.2021.064

Zhang, C., Xue, M., Zhu, K. & Yu, X. (2023) Climatology of significant tornadoes within China and comparison of tornado environments between United States and China. *Monthly Weather Review*, 151, 465–484. Available from: https://doi.org/10.1175/MWR-D-22-0070.1

Zheng, Y. (2020) Review of climatology and favorable environ mental conditions of tornado in China (in Chinese with English abstract). *Advances in Meteorological Science and Technology*, 10, 69–75.

Zhou, R., Meng, Z. & Bai, L. (2021) Differences in tornado activities and key tornadic environments between China and the United States. *International Journal of Climatology*, 42(1), 367–384. Available from: https://doi.org/10.1002/joc.7248

Zhou, X., Wang, X., Yu, X. & Fei, H. (2012) Application of excess rotation kinetic energy in distinguishing the tornadic and non-tornadic mesocyclones in China (in Chinese with English abstract). *Plateau Meteorology*, 31, 137–143.

SUPPORTING INFORMATION

Additional supporting information can be found online in the Supporting Information section at the end of this article.

How to cite this article: Zhang, R., Xue, M. & Yu, X. (2025) Environments of tornadic and non-tornadic supercells in China and optimized significant tornado parameter for China region. *Quarterly Journal of the Royal Meteorological Society*, e5027. Available from: https://doi.org/10.1002/qj.5027